Rapid SARS-CoV-2 Adaptation to Available Cellular Proteases

M. Zeeshan Chaudhry[1,10,*], Kathrin Eschke[1,10], Markus Hoffmann[2,3], Martina Grashoff[4], Leila Abassi[1], Yeonsu Kim[1], Linda Brunotte[5], Stephan Ludwig[5], Andrea Kröger[4,6], Frank Klawonn[7,8], Stefan Pöhlmann[2,3], Luka Cicin-Sain[1,9,*]

[1]Department of Vaccinology and Applied Microbiology, Helmholtz Centre for Infection Research, Braunschweig, Germany.

[2]Infection Biology Unit, German Primate Center, Göttingen, Germany.

[3]Faculty of Biology and Psychology, Georg-August-University Göttingen, Göttingen, Germany.

[4]Research Group Innate Immunity and Infection, Helmholtz Centre for Infection Research, Braunschweig, Germany.

[5]Institut für Virologie (IVM), Westfälische Wilhelms-Universität Münster, Münster, Germany.

[6]Institute of Medical Microbiology and Hospital Hygiene, Otto von Guericke University, Magdeburg, Germany

[7]Biostatistics Group, Helmholtz Centre for Infection Research, Braunschweig, Germany.

[8]Department of Computer Science, Ostfalia University, Wolfenbüttel, Germany.

[9]Centre for Individualized Infection Medicine (CIIM), Hannover, Germany.

[10]These authors contributed equally.

*Correspondence: zeeshan.chaudhry@helmholtz-hzi.de (M.Z.C), luka.cicin-sain@helmholtz-hzi.de (L.C.-S.)

Classification

Biological Sciences, Microbiology;

Keywords

SARS-CoV-2; Furin Cleavage Site; Coronavirus spike priming; Spike Mutation; Deep Sequencing;

Author Contributions

Conceptualization, M.Z.C.; Methodology, M.Z.C., K.E., M.H. and F.K.; Software and Formal Analysis, M.Z.C., K.E., M.H. and F.K.; Investigation, M.Z.C., K.E., M.H., M.G., L.A. and Y.K.; Data Curation, M.Z.C.; Writing – Original Draft, M.Z.C., K.E. and L.C.-S.; Writing – Review & Editing, M.Z.C., K.E., M.H., L.B., S.L., A.K., and L.C.-S.; Supervision, A.K. S.P., and L.C.-S.; Resources, L.B., and S.L.; Funding Acquisition, S.P. and L.C.-S.

1 **ABSTRACT**

2 Since the pandemic spread of SARS-CoV-2, the virus has exhibited remarkable genome

3 stability, but recent emergence of novel variants show virus evolution potential. Here we show

4 that SARS-CoV-2 rapidly adapts to Vero E6 cells that leads to loss of furin cleavage motif in

5 spike protein. The adaptation is achieved by asymptotic expansion of minor virus

6 subpopulations to dominant genotype, but wildtype sequence is maintained at low percentage

7 in the virus swarm, and mediate reverse adaptation once the virus is passaged on human lung

8 cells. The Vero E6-adapted virus show defected cell entry in human lung cells and the mutated

9 spike variants cannot be processed by furin or TMPRSS2. However, the mutated S1/S2 site is

10 cleaved by cathepsins with higher efficiency. Our data show that SARS-CoV-2 can rapidly

11 adapt spike protein to available proteases and advocate for deep sequence surveillance to

12 identify virus adaptation potential and novel variant emergence.

13 **Significance Statement**

14 Recently emerging SARS-CoV-2 variants B1.1.1.7 (UK), B.1.351 (South Africa) and B.1.1.248

15 (Brazil) harbor spike mutation and have been linked to increased virus pathogenesis. The

16 emergence of these novel variants highlight coronavirus adaptation and evolution potential,

17 despite the stable consensus genotype of clinical isolates. We show that subdominant variants

18 maintained in the virus population enable the virus to rapidly adapt upon selection pressure.

19 Although these adaptations lead to genotype change, the change is not absolute and genome

20 with original genotype are maintained in virus swarm. Thus, our results imply that the relative

21 stability of SARS-CoV-2 in numerous independent clinical isolates belies its potential for rapid

22 adaptation to new conditions.

23 **INTRODUCTION**

24 Coronavirus disease COVID-19 emerged from Wuhan city in December 2019 and since has

25 killed more than 2.6 million people worldwide. The pandemic spread of the disease that

26 affected all human societies was found to be caused by a novel beta coronavirus, called severe

2

1   acute respiratory syndrome coronavirus 2 (SARS-CoV-2), which is closely related to severe

2   acute respiratory syndrome coronavirus (SARS-CoV)(1, 2). The typical, crown-like appearance

3   of the CoVs is attributed to homotrimers of spike (S) protein (3), which mediate binding to the

4   host cell receptors and subsequent membrane fusion. The CoV S protein can be subdivided

5   into two functional subunits: S1 and S2 (4). In case of SARS-CoV-2, the S1 subunit directly

6   binds to angiotensin-converting enzyme 2 (ACE2), which has been identified as the cellular

7   receptor for SARS-CoV and SARS-CoV-2 (5, 6). Upon ACE2 binding, S needs to be primed

8   by cellular proteases that leads to cleavage at the S1/S2 junction and the S2' site (5, 7). This

9   exposes the fusion peptide in the S2 subunit, allowing the fusion of viral and cellular

10   membranes.

11   CoVs can enter the cell by fusing the virus envelope with either the endosomal or the

12   cytoplasmic membrane, depending on the localization and availability of the cellular proteases

13   in the host cell. Hence, cellular proteases have a direct impact on the cellular tropism and

14   pathogenesis of CoVs. Different CoVs have evolved multiple ways to achieve proteolytic

15   priming. A wide diversity of cellular proteases, including trypsin, endosomal cathepsins,

16   transmembrane serine proteases (e.g., TMPRSS2) and furin are known to be involved in the

17   priming of CoV spike (7). The SARS-CoV-2-S protein harbors a multibasic cleavage site at

18   S1/S2, as opposed to the monobasic site that is present in the SARS-CoV-S (5). The multibasic

19   site at S1/S2 also constitutes a putative furin cleavage site (RRAR). The consensus sequence

20   for furin cleavage site is widely described as R-X-K/R-R↓ (8, 9). The S protein of numerous

21   betacoronaviruses can be activated by furin at S1/S2 site; here, furin typically recognizes and

22   cleaves at RRXRR motif (7, 10). SARS-CoV and murine hepatitis virus strain 2 (MHV-2) are

23   two prominent exceptions of the betacoronavirus family that lack a furin cleavage site and need

24   to be cleaved by other cellular proteases (7).

25   Interestingly, the furin recognition sequence present in SARS-CoV-2 S is identical (however,

26   in opposite orientation) to the putative heparan sulfate (HS) interaction consensus sequences

27   (XBBXBX, where B is a basic amino acid) (11). It has been shown that cell culture adapted

1   Sindbis virus can mediate attachment to cell surface HS via furin cleavage site (8). Similarly,

2   upon *in vitro* culturing, CoVs often exhibit a tradeoff between the furin cleavability of S protein

3   and HS binding (10, 12). Thus, some CoVs can adapt to use HS as entry receptor in cultured

4   cells (12). Recently, SARS-CoV-2 mutants with deletions at the S1/S2 junction have been

5   described to emerge upon culturing the virus in Vero E6 cells (13). Clinical SARS-CoV-2

6   isolates, identified during the course of the current pandemic, have shown remarkably few

7   mutations in the consensus sequence (14). However, several newly emerged SARS-CoV-2

8   variants seem to harbor mutations in S protein and exhibit increased transmission. For

9   instance, the SARS-CoV-2 variant B.1.1.7 that emerged in the United Kingdom has been

10   associated with a surge of COVID-19 cases (15).

11   In order to understand the dynamics of SARS-CoV-2 adaptation, we serially passaged virus

12   strains in defined cell types and controlled environment. We show that SARS-CoV-2 rapidly

13   adapts to culture conditions, by natural selection of pre-existing subdominant population in

14   virus swarm. Furthermore, we show that the loss of the furin cleavage motif in Vero cells is due

15   to a selection for virus variants with S protein optimized for efficient cleavage with cathepsins.

16   However, viruses with the intact motif are retained as subdominant population in the swarm.

17   Therefore, re-passaging of such mutated swarms on cells expressing TMPRSS2 results in a

18   prompt reversion to the original genotype observed in low-passage clinical isolates.

19   **RESULTS**

20   **SARS-CoV-2 rapidly adapted upon culture on Vero E6 cells**

21   We performed deep sequencing of minimally passaged SARS-CoV-2 isolates to investigate

22   the genome diversity and presence of minor variants. We observed considerable diversity in

23   Ischgl (NK) and locally isolated Braunschweig (Br) strain that have been passage in vitro for

24   four and 2 passages, respectively (Figure 1A-B). NK-P4 showed around 12 thousand

25   nucleotide positions (12,406) with minor variants at more than 0.1% frequency and 1244

26   positions with >1% mutation frequency. Similarly, Br-P2 had 13,211 and 1175 positions with

27   >0.1% and >1% mutation frequency, respectively. In order to exclude that the observed

1   diversity is due to in vitro passaging, we also analyzed publically available SARS-CoV-2 RNA-

2   Seq data (GSA accession number CRA002390) from bronchoalveolar lavage (BAL)(16).

3   SARS-CoV-2 sequence from two patients showed high diversity similar to our minimally

4   passaged isolates. Patient one sequence had 17410 positions with >0.1% and 2163 with >1%

5   mutation as compared to consensus genotype, while SARS-CoV-2 genome from patient two

6   had 6920 positions with >0.1% mutation frequency and 1161 positions with >1% allele

7   frequency. On the other hand, BAC derived SARS-CoV-2 clone has been shown to possess

8   relatively low diversity and lower number of genome position with >1% mutation frequency

9   (17). These data suggested that SARS-CoV-2 virus quasispecies diversity despite stable

10   consensus genotype.

11   Sequence analysis of different SARS-CoV-2 clinical isolates passaged on Vero E6 cells

12   revealed point mutation at virus genome position 23,607, which results in the loss of the furin

13   cleavage site PRRARS at S1/S2 junction region (Table S1). These observations are in line

14   with previous publications (13, 18). To understand how fast such mutations occur, we

15   sequenced genomes of SARS-CoV-2 clinical isolates that were serially passaged on Vero E6

16   cells. Overall, the SARS-CoV-2 genomes were stable after multiple passages. However, we

17   observed a very rapid onset of mutations in the furin recognition motif at S1/S2 site upon

18   passaging in Vero E6 cells (Figure 1A-B). The Ischgl (NK) strain developed multiple point

19   mutations at the furin cleavage site, resulting in loss of arginine in S protein position 682 and

20   685 (Figure 1A, 1C). NK strain also showed emergence of other mutation in spike with low

21   frequency of mutated population, these are N148K (11.59%) and H245R (16.26%) in NK-P8

22   after eight passages in Vero E6 cells (Figure 1A). The mutation frequency for N148K and

23   H245R increased in NK-P12 to 64.11% and 19.25% respectively (Figure S2). These S

24   mutations were not observed in other tested strains. We used the local Braunschweig (Br)

25   isolate to compare the dynamics of S1/S2 site mutation, as we had access to earlier passages

26   of the Br strain. Here, a more rapid change in the composition of viral population was observed,

27   where >85% of passage 3 (P3) genomes showed R682W mutation in S protein (Table S1;

28   Figure S1A). We used the South Tyrol (FI) strain to compare the nature of mutation at the furin

1   cleavage site and observed a single point mutation (R682W) in the RRAR site (Figure S1C),

2   which was similar to Br strain. Rapid mutation in the furin site was accompanied with retention

3   of a small fraction of genomes with wildtype furin site in all strains (Table S1). For instance,

4   NK strain showed ~8.35% genomes with intact wildtype furin site after 12 passages in Vero

5   E6 (Figure S2).

6   A mathematical model was used to fit a non-linear curve to observed mutation frequency data

7   and calculate the rate of mutation frequency change at the furin cleavage site (Figure 1D). The

8   NK strain showed presence of multiple sub-species including three major variants with

9   mutation at position 23,606, 23,607 and 23,616 (Figure S1D). Thus, we summed the mutation

10   frequencies of these three positions to model the change in mutation frequency. For NK strain,

11   the rate was calculated as 0.3 (change in mutation frequency/day). The Br strain mutated at a

12   much higher rate of 0.81 per day (Figure S1B). We attributes this to the high mutation

13   frequency present in the Br strain (Br-P2).

14   Overall, the data demonstrated that the S1/S2 furin cleavage site was rapidly mutated upon

15   SARS-CoV-2 culture in Vero E6 cells, but it was not completely lost and virus genomes with

16   wildtype furin site were retained as subdominant variant in the population.

17   **High passage SARS-CoV-2 strains showed improved growth on Vero E6 but impaired**

18   **growth on Calu-3 cells**

19   In order to understand if the observed mutations in S influence viral growth, we compared the

20   cell-to-cell virus spread on Vero E6 cells by assessing plaque sizes. At 3 days post infection

21   (dpi), a significant increase in plaque sizes of high-passage virus in three independently

22   passaged virus strains was observed (Figure 2A-B). To validate the results independently, we

23   performed multi-step virus growth kinetics of two different virus isolates in Vero E6 cells and

24   noticed that in both cases the high-passage virus showed significantly higher titers at 24h post

25   infection (Figure 2C). We considered the possibility that the high-passage virus could be more

26   efficiently released from infected cells, and compared virus titers in infected cells lysates

27   (Figure 2D). In both conditions, the high-passage viruses showed higher titers early upon

6

1   infection. Therefore, we concluded that the growth advantage of high-passage virus was a

2   result of an early event that occurred before virus release.

3   To ascertain the growth properties of Vero-passaged virus on cells expressing TMPRSS2, we

4   tested the growth of virus strains on Calu-3 cells, and observed a mirror image of growth

5   properties observed in Vero E6 cells. The low passage viruses grew substantially better at

6   early time points post infection and the effects were observable equally in cell lysates and in

7   the supernatants (Figure 2E-F). These results agree with the previous report that a multibasic

8   cleavage site in the S protein is necessary for priming by TMPRSS2 (19).

9   **SARS-CoV-2 rapidly restored the furin cleavage site upon passage on TMPRSS2+ cells**

10   The low passage virus growth in Calu-3 cells suggested that the furin cleavage site confers

11   growth advantage in these cells and may result in selection of SARS-CoV-2 genomes with

12   wildtype furin site. Therefore, we took the NK strain that had been passaged 6 times in Vero

13   E6 cells (NK6), and re-passaged it on Calu-3 cells. SARS-CoV-2 genomes with wildtype furin

14   site were present as a subdominant fraction (~15%) in the NK6 viral population. Upon four

15   passages in Calu-3 cells, we observed a substantial reversion to the wildtype sequence with

16   the intact furin site (>97%) (Figure 3A). A similar reversion was observed upon passaging the

17   virus on Caco-2 cells: the sequence changed to a functional furin cleavage site in the vast

18   majority of viral genomes (>95%). While high-passage viruses showed growth disadvantage

19   in Calu-3 cells early upon infection, the virus titers rapidly recovered to low-passage levels

20   (Figure 2E-F). The data suggest that high-passage viruses rapidly changed consensus

21   genotype back to wildtype in Calu-3 cells. Thus, to understand the kinetics of the reversion,

22   the virus was sequenced after each sequential passages on Calu-3. Interestingly, the majority

23   of the reversion occurred already by on passage (Figure 3B), but a fraction of genomes with

24   the mutated cleavage site was retained as subdominant population in the virus swarm. The

25   composition of NK6 virus population was reshaped at reversion rate of 0.63 (change in

26   mutation frequency/day)(Figure 3C). The consensus sequence of low-passage viruses was

27   unaltered by their passaging on Calu-3 or Caco-2 cells (Figure 3D; Figure S3A). While S1/S2

1   site mutant genomes were present at a low level, their frequency did not change. The rate of

2   mutation frequency change suggested that the furin site mutations in both directions were a

3   result of targeted adaptation, rather than drift. Furthermore, all viruses passaged on Calu-3

4   cells showed a highly similar and stable population composition, regardless of the underlying

5   mutations induced by prior passaging on Vero cells. On the other hand, hitherto unreported

6   mutations L27S and E-T30I in the envelope (E) protein occurred upon virus passaging in Calu-

7   3 and in Caco-2 cells (Figure S3B-C; Table S2).

8   **Role of the SARS-CoV-2-S furin cleavage site in cell entry**

9   Cellular proteases are critical for SARS-CoV-2 cell entry and their availability affects the virus

10   tropism (5). Therefore, to test the role of different proteases, we infected Vero E6, Calu-3 and

11   Caco-2 cells with low and high-passage viruses in presence of a TMPRSS2 inhibitor

12   (camostat), a furin inhibitor (FI), or a broad-spectrum inhibitor of endosomal proteases (E-64d).

13   The growth of all virus strains was inhibited by E-64d on Vero E6 cells, but not by camostat or

14   FI, alone or in combination (Figure 4A). The combined use of E-64d and other protease

15   inhibitors did not depress virus titers over the values observed in cells treated with E-64d alone

16   (Figure S4A). This suggests that endosomal proteases, but not the cell-surface ones, were

17   crucial for SARS-CoV-2 replication in Vero E6 cells. Importantly, no difference in titer between

18   the high and the low-passage virus was observed in the presence of E-64d, arguing that the

19   effect of the mutation in the high-passaged virus might occur during virus entry.

20   An inverse phenotype was observed in Calu-3 cells, where the TMPRSS2 inhibitor reduced

21   the growth of all tested viruses, whereas E-64d and FI showed a less pronounced effect (Figure

22   4B). The differences in virus titers, seen in untreated controls, were erased in the presence of

23   camostat. Finally, virus growth in presence of all three inhibitors was entirely abrogated in

24   Calu-3 cells (Figure S4A). Virus replication in Caco-2 cells was not affected by inhibition of one

25   type of protease alone, but combinations of protease inhibitors resulted in reduction of virus

26   titers (Figure 4C). Although at 48 hpi the growth of low and high-passage viruses was similar

1 in untreated controls, the pattern of virus growth reduction in the presence of protease

2 inhibitors was similar to 24 hpi (Figure S3B-D).

3 These data suggested that growth defect of high passage SARS-CoV-2 strain is likely due to

4 reduced entry of mutated S variants in TMPRSS2$^+$ cells. We generated VSV pseudotyped virus

5 particles that harbor wildtype SARS-CoV-2-S with PRRARS sequence at S1/S2 site, and

6 variants with P**W**RARS or PRRA**H**S S1/S2 site sequence, two major mutated S variants that

7 were detected in majority of passaged strains. We analyzed the VSV pseudovirus entry in Vero

8 E6, Calu-3 and Caco-2 cells to ascertain the role of furin cleavage site in S priming and cell

9 entry process. Viruses harboring mutated SARS-CoV-2-S showed enhanced entry in Vero E6

10 cells, but the entry of these variants in Calu-3 and Caco-2 was substantially lower than wildtype

11 SARS-CoV-2-S virus (Figure 5). We concluded that the growth differences of passaged SARS-

12 CoV-2 in different cell lines is due to the presence of mutated S1/S2 site that modulate the

13 virus entry in these cells.

14 **Mutated S1/S2 site is not cleaved by furin and hampers efficient cell-cell fusion**

15 We have previously shown that PRRARS motif present at S1/S2 site of SARS-CoV-2-S

16 matches furin consensus sequence RX[K/R]R and can be efficiently cleaved by furin, and the

17 cleavage is inhibited with furin inhibitor (19). Here we show that mutated S proteins with

18 PWRARS or PRRAHS sequence were not primed by furin, although wildtype variant was

19 efficiently cleaved (Figure 5B). We next investigated if the mutated S can mediate syncytia

20 formation in A549 cells, a cell type that has low expression of furin (20). We co-transfected

21 cells with plasmids that expressed DsRed and S protein and observed that wildtype S protein

22 expression resulted in multi-nucleated giant cell formation (Figure 5C), likely due to low furin

23 expression in A549 cells. Mutated S proteins showed very few small syncytia in the absence

24 of trypsin treatment, although trypsin treatment increase syncytia size for all conditions. Lastly,

25 we show that TMPRSS2 expression enhanced cell-cell fusion by wildtype S protein, but the

26 mutated S proteins could not be processed by TMPRSS2 to increase syncytia formation. The

27 lack of syncytia formation by mutated S proteins indicated that high passage SARS-CoV-2

9

1   strains with high mutation frequency have limited cell-cell spread and likely spread via free

2   virus particles.

3   **Heparan sulfate antagonist did not inhibit SARS-CoV-2 adaptation in Vero E6 cells**

4   It has been previously reported that CoVs may trade furin cleavage sites in cell culture for a

5   heparan sulfate (HS) binding site, thus improving virus binding to the cell surface (10, 12).

6   However, in the case of SARS-CoV-2, the furin site PRRARS has a composition that overlaps

7   with the HS binding motif XBBXBX. The observed mutations in HS binding motif (R682W and

8   R685H) decreased the positive charge of the site and increased its hydrophobicity. We

9   hypothesized that virus is mutating S1/S2 site to lose the HS binding site in the S protein, thus

10   enhancing the growth of mutated virus in TMPRSS2$^-$ Vero E6. To test this hypothesis, we

11   compared the growth of the low-passage virus to the high-passage mutants with HS antagonist

12   in Vero E6 cells. At 24 hpi, we observed a 10-fold median increase in virus titers of the low-

13   passage virus in the presence of HS antagonist, but the effect on high-passage viruses was

14   non-significant (Figure 6A). HS antagonist treatment increased the virus plaque size, but the

15   difference between low and high-passage virus remained significant (Figure 6B; Figure S5B).

16   Furthermore, absorbing the virus on soluble or immobilized heparin resulted in a modest

17   decrease in virus infectiousness of the low-passage virus, but no effects on the high-passage

18   one (Figure S5A). We argued that modest HS antagonist effects might inhibit SARS-CoV-2

19   adaptation in the Vero E6 cells. Thus, we passaged the viruses in the presence of surfen and

20   sequenced the genome after four passages. However, we observed that all three strains

21   passaged in the presence of HS antagonist mutated the S1/S2 site (Figure 6C; Figure S5C-

22   D). The data indicate that although HS antagonist modestly influence the growth of low-

23   passage SARS-CoV-2 virus, heparan sulfate binding does not derive SARS-CoV-2 adaptation

24   in Vero E6 cells.

25   **SARS-CoV-2 S1/S2 site adaption to available proteases**

26   We next investigated for possible optimization of S1/S2 cleavage site in a protease specific

27   manner. We used SARS-CoV-2-S S1/S2 site derived peptides that were fluorescently labeled

1 with FAM-TAMRA FRET pair to assess the peptide cleavage efficiency by different proteases

2 (Figure 7A). The wildtype SARS-CoV-2-S S1/S2 site harboring furin cleavage site was rapidly

3 cleaved by furin, but the mutated peptides with PWRARS or PRRAHS sequence were not

4 cleaved by furin (Figure 7B). This confirmed the VSV pseudotyped virus priming observed with

5 western blot analysis (Figure 5B). The peptide cleavage kinetics showed that mutated peptide

6 with PWRARS S1/S2 site was processed at a high rate by recombinant cathepsins, and

7 PRRAHS variant was efficiently cleaved by cathepsins B. Interestingly, trypsin processed the

8 PWRARS peptide with higher efficiency than the wildtype variant (Figure 7C). We concluded

9 that high passage SARS-CoV-2-S is more efficiently cleaved by cathepsins, which are

10 important for virus cell entry and S priming in Vero E6 cells. Thus, selection for SARS-CoV-2-

11 S variant more efficiently primed by cathepsins derived virus adaptation in Vero E6 cells and

12 lead to the emergence of S1/S2 site mutants in these cells.

13 **DISCUSSION**

14 RNA virus populations are composed of a cloud of different genome variants known as

15 quasispecies (21, 22) that arise due to erroneous proof-reading of RNA-dependent RNA

16 polymerase (RdRp), and are essential for adaptive evolution and fitness of RNA viruses (23).

17 Our deep sequencing data showed that SARS-CoV-2 exhibit remarkable genome stability

18 overall. However, this stability does not hinder the ability of the virus to adapt quickly.

19 Furthermore, high diversity in the clinical SARS-CoV-2 isolates as compared to BAC derived

20 clones suggest that these minor variants play an important role in overall virus fitness and its

21 adaptation potential (17).

22 Although the loss of furin site led to virus growth advantage in Vero E6 cells, genomes with

23 wildtype motif were not completely lost. The virus population accumulated the mutations at the

24 furin cleavage site in an asymptotic manner, stabilizing after 4-5 passages and maintaining a

25 subdominant fraction of population with the intact motif. Mutation dynamics in Calu-3 cells

26 followed a similar, albeit reverse, pattern and viruses with mutated PRRARS motif were

27 retained in the virus swarm. We observed different adaptation rate in different strain that

1   positively co-relates with the size of the subdominant population in these strains, which

2   indicates that adaptation dynamics are likely dependent on the presence and size of

3   subdominant populations in virus swarm. Furthermore, absence of S1/S2 mutation in BAC

4   derived SARS-CoV-2 clones after five passages in Vero E6 cells (17) suggest that the rapid

5   emergence of mutation that we observed is likely due to the presence of minor variants in

6   clinical isolates. These observations suggest that SARS-CoV-2 maintains a considerable

7   diversity in the quasispecies, facilitating natural selection and a rapid virus adaptation to

8   changing environment and conditions. The imperfect fitness at individual level adds to the

9   ability of the population to quickly adapt, thus contributing to the overall fitness of the swarm.

10 Our results are in agreement with previous report that the presence of a multibasic site is

11 necessary for spike processing by furin and TMPRSS2 (19). In PRRAHS site, the arginine at

12 position 685 is replaced by another basic amino acid histidine, and the ratio of hydrophilic

13 residues change from 67% to 50%. Although PRRAHS fulfills multibasic site criteria, arginine

14 is required at position 685 for TMPRSS2 spike priming. It is unclear if the PRRAHS site is

15 cleaved at histidine or one of the other arginine residues.

16 The growth advantage on Vero E6 cells was surprising, because the furin cleavage site should

17 have provided an advantage to viruses on cells that express furin or TMPRSS2 enzymes

18 (Calu-3 or Caco-2), but its absence should not confer growth advantage in cells that lack these

19 enzymes. SARS-CoV-2 furin cleavage site PRRARS has a composition that overlaps with the

20 HS binding motif XBBXBX, and HS binding in the absence of cleavage enzymes might exert

21 selection pressure. However, the importance of these HS binding receptors *in vivo* is debated

22 as many viruses acquire HS binding upon cell culture adaptation (24). The SARS-CoV-2-S

23 protein has been shown to bind HS (25) and heparin was shown to inhibit SARS-CoV-2

24 infection *in vitro* (26). Furthermore, Kim et al. has identified PRRARS site in the SARS-CoV-2

25 S protein as a putative HS binding site using an unbiased ligand-docking model (25). We report

26 that the putative HS binding motif influence the growth of SARS-CoV-2, but virus adaptation is

27 not affected by HS antagonists. Instead, the virus adaptation is driven by selection of S1/S2

1 variants that can be more efficiently cleaved by cathepsins, which are responsible for spike

2 priming and virus entry in Vero E6 cells. The reverse adaptation to original genotype in Calu-

3 3 cells is likely due to TMPRSS2 dependent priming, since these cells do not express robust

4 levels of cathepsin L (27). However, the reverse adaptation in the Caco-2 cells show that

5 priming and processing by TMPRSS2 is preferred over cathepsins.

6 Our study suggest that clinical SARS-CoV-2 isolates should be sequenced with deep

7 sequencing to cover the minor genome variants present in the virus swarm instead of solely

8 focusing on consensus genotype. The emergence of the novel SARS-CoV-2 variants highlight

9 that virus can mutate and these novel variants show enhanced entry in human lung cells (28).

10 Furthermore, these variants show reduced neutralization by serum from convalescent patient

11 or vaccinated individuals. Out results argue that it is likely that these variants were present as

12 minor subpopulations and expanded because of selection pressure. However, it is unclear if it

13 purely to enhance virus entry in host cells or if is to evade the humoral immune response.

14 Overall, we demonstrate a high potential of SARS-CoV-2 rapid adaptation, due to its swarm-

15 like replication. Future research in animal models shall explore the potential for the *in vivo*

16 adaptation of SARS-CoV-2, the quasispecies diversity and the bottlenecks imposed on the

17 virus spread. Our research indicates that the presence of subdominant genetic variants within

18 SARS-CoV-2 isolates needs to be considered as a potential determinant of their virulence.

19 **MATERIALS AND METHODS**

20 **Cell cultures and Viruses**

21 Vero E6 (ATCC CRL-1586), and 293T (DSMZ ACC-635) cells were maintained in DMEM

22 medium supplemented with 10% fetal calf serum (FCS), 2 mM L-glutamine, 100 IU/mL

23 penicillin and 100 μg/mL streptomycin. Calu-3 (ATCC HTB-55) and Caco-2 (ATCC HTB-37)

24 were cultured in Eagle's Minimum Essential Medium (EMEM) supplemented with 10% FCS, 2

25 mM L-glutamine, 100 IU/mL penicillin, 100 μg/mL streptomycin and 1x non-essential amino

26 acid solution (Gibco MEM Non-Essential Amino Acids Solution 100X). A549 (ATCC CCL-185)

13

1   cells were incubated in DMEM/F-12 medium with Nutrient Mix (ThermoFisher Scientific). All

2   incubations of cells and virus were at 37 °C in a 5% CO_2 atmosphere.

3   The SARS-CoV-2 strains used in the study are Braunschweig isolate (hCoV-19/Germany/Br-

4   ZK-1/2020, GISAID database ID: EPI_ISL_491115), South Tyrol isolate (hCoV-

5   19/Germany/Muenster_FI1103201/2020, GISAID database ID: EPI_ISL_463008), Ischgl

6   isolate (hCoV-19/Germany/NK1103201/2020) and Zagreb isolate (hCoV-19/Croatia/ZG-297-

7   20/2020, GISAID database ID: EPI_ISL_451934).

8   **SARS-CoV-2 passage and virus stock generation**

9   Braunschweig isolate (Br) was derived from an oropharyngeal swab using Vero E6 cells. Zagreb

10 isolate (Zg) was isolated in Zagreb and received as passage 2 after propagation in Vero E6 cells.

11 Ischgl (NK) and South Tyrol (FI) strains were isolated by Stephan Ludwig lab in Muenster.

12 Passage 2 of NK, FI and Zg strains were further propagated by passaging twice in Vero E6

13 cells at low MOI (multiplicity of infection) to obtain working virus stocks. For serial passaging

14 of SARS-CoV-2 strains, Vero E6, Calu-3 and Caco-2 cells were seeded in T25 or T75 flask

15 one day before infection. Confluent monolayers of the cells were infected with virus and virus

16 supernatant was collected three days post infection (dpi) to further passage the virus.

17 Virus stocks were generated in a two-step protocol, where seeding stock was generated by

18 infecting one T75 flask of Vero E6 cells. The seeding stock virus supernatant was collected 3

19 dpi and used to infect 10 T75 flasks for virus stock generation. The virus stock supernatant

20 was collected from all flasks at 3 dpi and spun at 3000 g for 10 minutes (min) to remove cell

21 debris. Then, the virus supernatant was concentrated using Vivaspin 20 concentrators

22 (Sartorius Stedim Biotech) by spinning at 6000 g for 30 min. The resulting virus stock was

23 aliquoted and stored at -80°C until further use.

24 **SARS-CoV-2 titration**

25 SARS-CoV-2 was titrated with virus plaque assay on Vero E6 cells. Virus stocks were serially

26 diluted in virus titration media (VTM, DMEM supplemented with 5% FCS, 2 mM L-glutamine,

14

1 100 IU/mL penicillin and 100 µg/mL streptomycin) and titrated on 24-well plates. The virus

2 inoculum was added on the Vero E6 cells and incubated at 37°C. After 1 h, the inoculum was

3 removed and the cell were overlaid with VTM supplemented with 1.5% carboxymethylcellulose

4 (medium viscosity, C9481, Sigma-Aldrich) and incubated at 37°C. The overlay was removed

5 from the cell at 3 dpi and the plates were fixed by submerging them in a tank of 6%

6 formaldehyde (methanol stabilized) for at least 1 h. The cell monolayer was stained with crystal

7 violet and the plaques were quantified by visual inspection with microscope. Virus

8 supernatants were titrated in a similar fashion on 96-well plates.

9 **Growth kinetics and plaque area measurement**

10 Vero E6, Calu-3 or Caco-2 were seeded in a well of a 96-well plate. Confluent monolayers

11 were infected with at an MOI of 0.001. After 1 h of infection at 37°C, the inoculum was removed

12 and replaced by normal media. Supernatants and infected cell lysates were collected at

13 different time points post infection and virus titer were determined as described above.

14 To analyze cell-to-cell spread of SARS-CoV-2, the virus plaque area was determined. Vero E6

15 seeded in a well of a 24-well plate were infected with 30 PFU of SARS CoV 2. After 1 h of

16 infection, the inoculum was removed and cells were overlaid with VTM supplemented with

17 1.5% carboxymethylcellulose (medium viscosity, C9481, Sigma-Aldrich) and incubated at

18 37°C. For testing the effect of HS antagonist, cells were pretreated with 10 µM surfen or 1

19 mg/mL lactoferrin for one hour at 37°C before infection, and infection was performed in the

20 presence of surfen or lactoferrin. Finally, after 1 h, the virus inoculum was removed and

21 monolayer was overlaid with VTM supplemented with 1.5% carboxymethylcellulose and 10 µM

22 surfen or 1 mg/mL lactoferrin. Cells were fixed with 6% formaldehyde 3 dpi and stained with

23 crystal violet. The plaque area was quantified using a Zeiss LSM 980 Microscope. The plaque

24 area was measured with help of ZEISS ZEN lite 3.0 (Blue edition), and plotted using GraphPad

25 Prism.

26 **SARS-CoV-2 infection in the presence of protease inhibitors and HS antagonists**

1   SARS-CoV-2 cell entry inhibition was tested by seeding Vero E6, Calu-3 or Caco-2 cells in 96-

2   well plates, one day before infection. On the day on infection, cell were treated with protease

3   inhibitors (E-64d, 10µM; camostat, 50 10µM; furin inhibitor, 10µM) or HS antagonists (10 µM

4   Surfen or 1 mg/mL lactoferrin) for 1 h at 37°C before virus infection. The infection was

5   performed in the presence of protease inhibitors or HS antagonists, and after 1 h infection at

6   37°C, the virus inoculum was removed and normal media supplemented with inhibitors or HS

7   antagonists was given to the cells. The virus supernatant was collected at 1 and 2 dpi and

8   titrated on Vero E6 cells as described in SARS-CoV-2 titration section.

9   For analyzing the heparin binding, SARS-CoV-2 suspension containing ~1000 PFU was

10 incubated with heparin sodium salt (100 µg/mL) for 1 h at 37°C. After incubation, the

11 suspension was titrated on Vero E6 cells in a 24-well plate format. Similarly, for testing the

12 ability of immobilized heparin to bind SARS-CoV-2, Heparin−biotin sodium salt was

13 immobilized on Pierce™ Streptavidin Coated Plates (Thermo Fisher Scientific). The volume

14 used to immobilize Heparin-biotin (100 µg/mL) was 100 µL per well. Plates were incubated at

15 37°C for 15 minutes and then washed three times with 1x PBS. The virus suspension (1000

16 PFU) was added to the heparin-coated wells along with empty streptavidin coated wells and

17 incubated for 1 h at 37°C. Afterwards, the suspension was titrated on Vero E6 cells in a 24-

18 well plate format.

19 **Pseudovirus Entry Assay**

20 We used vesicular stomatitis virus (VSV) pseudotyped with SARS-CoV-2 S that were used

21 according to a published protocol (29). In brief, 293T cells were transfected with expression

22 plasmids for SARS-CoV-2 S proteins of either wildtype Wuhan/Hu-1/2019 (lineage B, with

23 D614G mutation inserted) or variants with mutation in furin cleavage site. At 24h post

24 transfection, the transfection medium was removed and cells were inoculated with a

25 replication-deficient VSV vector lacking the genetic information for the VSV glycoprotein (VSV-

26 G) and instead coding for an enhanced green fluorescent protein and firefly luciferase from

27 independent transcription units, VSV*ΔG-FLuc (kindly provided by Gert Zimmer, Institute of

1   Virology and Immunology, Mittelhäusern, Switzerland)(30). Following 1h of incubation at 37°C

2   and 5% CO2, the inoculum was removed and cells were washed with PBS, before culture

3   medium containing anti-VSV-G antibody (culture supernatant from I1-hybridoma cells; ATCC

4   CRL-2700) was added and cells were further incubated. The pseudotype virus particles were

5   harvested at 16-18 hpi. The culture medium was collected, centrifuged (2,000 g, 10 min, RT)

6   to pellet cellular debris and the clarified supernatant was transferred into fresh tubes and stored

7   at -80°C until further use. Each batch of pseudotypes was pre-tested for comparable

8   transduction efficiencies by the respective S proteins and absence of transduction by bald

9   control particles before being used. Furthermore, for each construct an untagged variant as

10   well as a version containing a C345 terminal HA epitope tag was constructed.

11   **Western blot analysis**

12   For the analysis of S protein processing, we subjected VSVpp harboring HA-tagged S proteins

13   to SDS-PAGE and Western blot analysis. For this, we loaded 1 ml VSVpp onto 50 µl of a 20

14   % (w/v) sucrose cushion and performed high-speed centrifugation (25.000 g, 120 min, 4°C).

15   Next, we removed 1 ml of supernatant, added 50 µl of 2x SDS-sample buffer and incubated

16   the samples for 15 min at 96°C. Thereafter, the samples were subjected to SDS-PAGE and

17   protein transfer to nitrocellulose membranes by Western blot. The membranes were

18   subsequently blocked in 5 % skim milk solution (PBS containing 0.05% Tween-20 [PBS-T] and

19   5 % skim milk powder) for 1 h at room temperature. The blots were then incubated over night

20   at 4 °C with primary antibody solution (all antibodies were diluted in PBS-T containing 5 %

21   skim milk; mouse anti-HA tag [Sigma-Aldrich, H3663, 1:2,500] or VSV matrix protein [Kerafast,

22   EB0011, 1:2,500]). Following this incubation, the blots were washed 3x with PBS-T before they

23   were incubated for 1 h at room temperature with peroxidase-coupled goat anti-mouse antibody

24   (Dianova, 115-035-003, 1:10,000). Finally, the blots were again washed and imaged. For this,

25   an in house-prepared enhanced chemiluminescent solution (0.1 M Tris-HCl [pH 8.6], 250

26   µg/mL luminol, 1 mg/mL para-hydroxycoumaric acid, 0.3 % H2O2) and the ChemoCam

1 imaging system along with the ChemoStar Professional software (Intas Science Imaging

2 Instruments GmbH) were used.

3 **Syncytium formation assay**

4 A549-ACE2 or A549-ACE2-TMPRSS2 cells were grown on coverslips seeded in 24-well plates

5 and co-transfected with DsRed vector (1 µg/well) and S protein expression plasmid (1 µg/well)

6 using Lipofectamine 2000 LTX with Plus reagent (Thermo Fisher Scientific) and OptiMEM

7 medium (Gibco). After 6 h, the transfection solutions were aspirated and the cells further

8 incubated for 24 h in standard culture medium. The medium was changed next day to serum

9 free medium with or without 1 µg/ml bovine trypsin (Sigma-Aldrich) and the cells were

10 incubated for additional 1 h at 37°C. Cells were washed with PBS and fixed with 4 %

11 paraformaldehyde solution for 20 min at room temperature. After fixation, cells were stained

12 with DAPI solution and analyzed by bright-field microscopy using a Zeiss LSM800 confocal

13 laser scanning microscope and the ZEN imaging software.

14 **Peptide Cleavage Assay**

15 Target cleavage peptides derived from the SARS-CoV-2 spike S1/S2 site amino acid

16 sequence TNSPRRARSVA and flanked with FAM-TAMRA FRET pair ([FAM]TNSPRRARSVA-

17 K[TAMRA][COOH.acetate]) were synthesized by Thermo Fisher Scientific. Wildtype peptide

18 TNSPRRARSVA along with two mutated peptides TNSPWRARSVA and TNSPRRAHSVA

19 harboring point mutation in amino acid sequence of furin cleavage site were synthesized.

20 Recombinant furin was purchased from New England Biolabs. Recombinant L-1-Tosylamide-

21 2-phenylethyl chloromethyl ketone (TPCK)-treated trypsin was obtained from Sigma-Aldrich.

22 Recombinant cathepsin B and cathepsin L were purchased from R&D Systems.

23 Florescent peptides were diluted to 25 µM and the cleavage reaction was performed in 100 µL

24 total volume. The reactions buffer was composed of 100 mM Hepes, 0.5% Triton X-100, 1 mM

25 CaCl2 and 1 mM 2-mercaptoethanol (pH 7.5) for furin (10 U/mL); PBS for trypsin (100 ng/mL);

26 25 mM MES, pH 5.0 for cathepsin B (100 ng/µL); 50 mM MES, 5 mM DTT, 1 mM EDTA,

27 0.005% (w/v) Brij-35, pH 6.0 for cathepsin L (100 ng/µL). Reactions were performed in

1   Varioskan Flash (Thermo Scientific) at 30 °C, and kinetic fluorescence measurements were

2   recorded at one minute interval for 60 min with λex 495 nm and λem 520 nm wavelengths

3   setting. Peptide cleavage efficiency was determined by calculating area under the curve (AUC)

4   with fold increase in FAM florescence over time (time t=10 min to t=40 min).

5   **SARS-CoV-2 RNA isolation and sequencing**

6   For the inactivation of SARS-CoV-2, the virus suspension was mixed 1:1 with peqGOLD

7   TriFast (VWR). Following, RNA was extracted using the innuPREP Virus RNA Kit (Analytik

8   Jena) according to the manufacturer's instructions. The RNA quality was confirmed with

9   Bioanalyzer (Agilent Technologies) and Qubit (Thermo Fisher Scientific). The sequencing

10 libraries were prepared using NEBNext Ultra II Directional RNA Library Prep Kit (New England

11 Biolabs) including ERCC RNA Spike-in control. The sequencing was performed with NovaSeq

12 6000 SP Reagent Kit (100 cycles) on NovaSeq 6000 System (Illumina).

13 Raw fastq files were processed to trim adaptor and low quality reads (fastp 0.20.0). The

14 resulting sequence reads were aligned with reference (BWA 0.7.8). The alignment file was

15 sorted (SAMtools version 1.10) and realigned (GATK IndelRealigner version 3.7). Finally,

16 pileup file (SAMtools) was created and mutation were detected with VarScan (version 2.3.9).

17 Mutation frequency for whole genome was calculated by extracting total read depth and

18 reference base reads for each nucleotide from pileup file using SAMtools, where mutation

19 frequency in the population is given as ratio of reference reads to total reads at the position.

20 Mutation frequencies were converted to percent values and plotted with ggplot2

21 (R/Bioconductor 4.0). Alignment files were inspected with IGV (version 2.8.3) and Tablet

22 (version 1.19.09.03) to access if nearby mutations in the furin cleavage site are present on

23 same reads.

24 **Mathematical modelling**

25 The mathematical model, to fit the curves for the mutation, assumes that the proportion of

26 viruses with a mutation on the considered chromosome (SARS-CoV-2 genome positions

1 23606, 23607 and 23616) at time t depends on the initial proportion of mutated viruses $y(0)$,

2 the mutation rate a and the reverse mutation rate b. This leads to the ordinary differential

3 equation $y' = a(1 - y) - by$ with the general solution $y(t) = ce^{-(a+b)t} + \frac{a}{a+b}$. Assuming

4 that there are no mutations at time zero, i.e. $y(0) = 0$, then $c = -\frac{a}{a+b}$ follows. If we start with

5 a mutated strain, i.e. $y(0) = 1$, this implies $c = \frac{b}{a+b}$. The mutation rates a and b of the

6 corresponding non-linear curve are estimated based on the data by the optimization procedure

7 optim provided by the R statistics software, minimizing the sum of absolute errors. R script

8 used is provided in supplemental data.

9 **QUANTIFICATION AND STATISTICAL ANALYSIS**

10 Kruskal-Wallis with Dunn's comparison and two-way analysis of variance (ANOVA) with

11 Dunnett posttest were used to test for statistical significance. Where appropriate, two-way

12 ANOVA with Sidak's multiple comparison was used. P-values < 0.05 were considered

13 significant (*p < 0.05; **p < 0.01; ***p < 0.001), ****p < 0.0001, p > 0.05 not significant (n.s.).

14 For all statistical analyses, the GraphPad Prism 7 software package was used (GraphPad

15 Software).

16 **DATA AND CODE AVAILABILITY**

17 The SARS-CoV-2 deep sequencing data generated during this study are available at NCBI

18 sequence read archive. (SRA accession: PRJNA650134;

19 https://www.ncbi.nlm.nih.gov/Traces/study/?acc=PRJNA650134). The R code used in this

20 study are provided in supplemental data (Data S1).

21 **MATERIALS AVAILABILITY**

22 Further information and requests for resources and reagents can be directed to M. Zeeshan

23 Chaudhry (Zeeshan.chaudhry@helmholtz-hzi.de) and Luka Cicin-Sain (luka.cicin-

24 sain@helmholtz-hzi.de). The materials will be made available upon receipt of a material

25 transfer agreement (MTA).

5   **Declaration of Interests**

6   The authors declare no competing interests.

REFERENCES

1. C. Wang, P. W. Horby, F. G. Hayden, G. F. Gao, A novel coronavirus outbreak of global health concern. *Lancet* **395**, 470-473 (2020).

2. N. Zhu *et al.*, A Novel Coronavirus from Patients with Pneumonia in China, 2019. *N Engl J Med* **382**, 727-733 (2020).

3. B. W. Neuman *et al.*, Supramolecular architecture of severe acute respiratory syndrome coronavirus revealed by electron cryomicroscopy. *J Virol* **80**, 7918-7928 (2006).

4. M. A. Tortorici, D. Veesler, Structural insights into coronavirus entry. *Adv Virus Res* **105**, 93-116 (2019).

5. M. Hoffmann *et al.*, SARS-CoV-2 Cell Entry Depends on ACE2 and TMPRSS2 and Is Blocked by a Clinically Proven Protease Inhibitor. *Cell* **181**, 271-280 e278 (2020).

6. F. Li, W. Li, M. Farzan, S. C. Harrison, Structure of SARS coronavirus spike receptor-binding domain complexed with receptor. *Science* **309**, 1864-1868 (2005).

7. J. K. Millet, G. R. Whittaker, Host cell proteases: Critical determinants of coronavirus tropism and pathogenesis. *Virus Res* **202**, 120-134 (2015).

8. W. B. Klimstra, H. W. Heidner, R. E. Johnston, The furin protease cleavage recognition sequence of Sindbis virus PE2 can mediate virion attachment to cell surface heparan sulfate. *J Virol* **73**, 6299-6306 (1999).

9. K. Nakayama, Furin: a mammalian subtilisin/Kex2p-like endoprotease involved in processing of a wide variety of precursor proteins. *Biochem J* **327 (Pt 3)**, 625-635 (1997).

10. C. A. de Haan *et al.*, Cleavage of group 1 coronavirus spike proteins: how furin cleavage is traded off against heparan sulfate binding upon cell culture adaptation. *J Virol* **82**, 6078-6083 (2008).

11. A. D. Cardin, H. J. Weintraub, Molecular modeling of protein-glycosaminoglycan interactions. *Arteriosclerosis* **9**, 21-32 (1989).

12. C. A. de Haan *et al.*, Murine coronavirus with an extended host range uses heparan sulfate as an entry receptor. *J Virol* **79**, 14451-14456 (2005).

13. S. Y. Lau *et al.*, Attenuated SARS-CoV-2 variants with deletions at the S1/S2 junction. *Emerg Microbes Infect* **9**, 837-842 (2020).

14. L. van Dorp *et al.*, Emergence of genomic diversity and recurrent mutations in SARS-CoV-2. *Infect Genet Evol* **83**, 104351 (2020).

15. K. Leung, M. H. Shum, G. M. Leung, T. T. Lam, J. T. Wu, Early transmissibility assessment of the N501Y mutant strains of SARS-CoV-2 in the United Kingdom, October to November 2020. *Euro surveillance : bulletin Europeen sur les maladies transmissibles = European communicable disease bulletin* **26** (2021).

16. Y. Xiong *et al.*, Transcriptomic characteristics of bronchoalveolar lavage fluid and peripheral blood mononuclear cells in COVID-19 patients. *Emerg Microbes Infect* **9**, 761-770 (2020).

17. K. Chiem *et al.*, Generation and Characterization of recombinant SARS-CoV-2 expressing reporter genes. *J Virol* 10.1128/JVI.02209-20 (2021).

18. A. D. Davidson *et al.*, Characterisation of the transcriptome and proteome of SARS-CoV-2 using direct RNA sequencing and tandem mass spectrometry reveals evidence for a cell passage induced in-frame deletion in the spike glycoprotein that removes the furin-like cleavage site. 10.1101/2020.03.22.002204 %J bioRxiv, 2020.2003.2022.002204 (2020).

19. M. Hoffmann, H. Kleine-Weber, S. Pohlmann, A Multibasic Cleavage Site in the Spike Protein of SARS-CoV-2 Is Essential for Infection of Human Lung Cells. *Mol Cell* **78**, 779-784 e775 (2020).

20. F. P. Tay, M. Huang, L. Wang, Y. Yamada, D. X. Liu, Characterization of cellular furin content as a potential factor determining the susceptibility of cultured human and animal cells to coronavirus infectious bronchitis virus infection. *Virology* **433**, 421-430 (2012).

21. R. Andino, E. Domingo, Viral quasispecies. *Virology* **479-480**, 46-51 (2015).

22

22. A. S. Lauring, R. Andino, Quasispecies theory and the behavior of RNA viruses. *PLoS Pathog* **6**, e1001005 (2010).

23. A. V. Borderia, K. Rozen-Gagnon, M. Vignuzzi, Fidelity Variants and RNA Quasispecies. *Curr Top Microbiol Immunol* **392**, 303-322 (2016).

24. V. Cagno, E. D. Tseligka, S. T. Jones, C. Tapparel, Heparan Sulfate Proteoglycans and Viral Attachment: True Receptors or Adaptation Bias? *Viruses* **11** (2019).

25. S. Y. Kim *et al.*, Characterization of heparin and severe acute respiratory syndrome-related coronavirus 2 (SARS-CoV-2) spike glycoprotein binding interactions. *Antiviral Res* 10.1016/j.antiviral.2020.104873, 104873 (2020).

26. P. S. Kwon *et al.*, Sulfated polysaccharides effectively inhibit SARS-CoV-2 in vitro. *Cell Discov* **6**, 50 (2020).

27. J. E. Park *et al.*, Proteolytic processing of Middle East respiratory syndrome coronavirus spikes expands virus tropism. *Proc Natl Acad Sci U S A* **113**, 12262-12267 (2016).

28. M. Hoffmann *et al.*, SARS-CoV-2 variants B.1.351 and B.1.1.248: Escape from therapeutic antibodies and antibodies induced by infection and vaccination. *bioRxiv* 10.1101/2021.02.11.430787, 2021.2002.2011.430787 (2021).

29. H. Kleine-Weber *et al.*, Mutations in the Spike Protein of Middle East Respiratory Syndrome Coronavirus Transmitted in Korea Increase Resistance to Antibody-Mediated Neutralization. *J Virol* **93** (2019).

30. M. Berger Rentsch, G. Zimmer, A vesicular stomatitis virus replicon-based bioassay for the rapid and sensitive determination of multi-species type I interferon. *PLoS One* **6**, e25858 (2011).

1 **FIGURE LEGENDS**

2 **Figure 1. SARS-CoV-2 rapidly adapts upon passage in cultured cells.**

3 (A-B) Serial passages of Ischgl (NK) and Braunschweig (Br) strain were analyzed with deep

4 sequencing to assess the composition of viral population upon passaging in Vero E6 cells.

5 Each symbol represents an individual nucleotide, and genomic positions (x-axis) with mutation

6 frequency >1% are plotted. Red arrows highlight the position of the furin cleavage site in the

7 genome. (C) The mutation frequency of nucleotides at furin cleavage site in SARS-CoV-2 S

8 are plotted on y-axis for NK and Br strains at different passage in Vero E6 cells. Three bars

9 represent the nucleotide codon triplet for each corresponding amino acid at the furin cleavage

10 site from genomic position 23,603 to 23,620 (x-axis). (D) The sum of mutation frequency at the

11 furin site position 23,606, 23,607 and 23,616 of NK strain serially passaged on Vero E6 cells

12 is plotted against time. The genomic positions correspond to Wuhan-Hu-1 isolate (GenBank

13 accession no: NC_045512).

14 **Figure 2. Growth properties of passaged SARS-CoV-2 strains in different cell lines.**

15 (A-B) Vero E6 cells were infected with different passages of SARS-CoV-2 strains and the

16 plaque size was measured 3 dpi. Panel A shows the area of virus plaque on Vero E6 cells,

17 and panel B shows representative images of two different wells infected with NK-P4 and NK-

18 P7. (C-D) Virus growth kinetics on Vero E6 cells were established by infecting the cells at an

19 MOI of 0.001. Supernatants (panel C) and cell lysates (panel D) were collected at indicated

20 time points and titrated on Vero E6 cells. (E-F) Calu-3 cells were infected at an MOI of 0.001.

21 Supernatants (panel E) and cell lysates (panel F) were collected at indicated time post infection

22 and titrated on Vero E6 cells. Data are representative of two independent experiments. Mean

23 and ±SEM are plotted. Each symbol in panel A represent one plaque and data are pooled from

24 multiple infected wells of two independent experiments. Panel C-F symbols represent

25 biological replicates. Statistical significance was calculated using one way ANOVA with

26 Bonferroni posttest. $**p < 0.01$, $****p < 0.0001$.

1 **Figure 3. SARS-CoV-2 population composition at furin cleavage site reverts to low**

2 **passage virus levels upon passage in TMPRSS2^{+} human cells.**

3 The mutation frequency of genomic position 23,603 to 23,620 (x-axis) in SARS-CoV-2 genome

4 corresponding to amino acid codon triplets at furin cleavage site are plotted in Panel A, B and

5 D. (A) NK strain passaged 6 time in Vero E6 cells (NK6) was serially passaged independently

6 on Calu-3 and Caco-2 cells. P0 vero represents the genome of input virus and P4 calu-3 and

7 P4 caco-2 are the viruses cultured on respective cells lines for 4 passages. (B) The change in

8 SARS-CoV-2 furin site mutations is shown by plotting the nucleotide mutation frequency of

9 NK6 virus upon serial passaging in Calu-3 cells. (C) The sum of mutation frequency at furin

10 site position 23,606, 23,607 and 23,616 of NK6 strain serially passaged on Calu-3 cells is

11 plotted against time. (D) NK strain passaged 4 time in Vero E6 cells (NK4) was serially

12 passaged on Calu-3 and Caco-2 cells. P0 vero represents the genome of low passage input

13 virus and P4 calu-3 and P4 caco-2 are the viruses cultured on Calu-3 and Caco-2 cell lines for

14 4 serial passages.

15 **Figure 4. Inhibition of low and high-passage SARS-CoV-2 strain growth by different**

16 **protease inhibitors.**

17 Vero E6 (A), Calu-3 (B) and Caco-2 (C) cells were infected at an MOI of 0.01 in the presence

18 of different protease inhibitors. The supernatant from infected cells was collected at 24 hpi and

19 titrated on Vero E6 cells. Data is representative of two independent experiments and error bars

20 represent ± SEM of three biological replicates. Statistical significance was calculated using

21 two-way ANOVA with Dunnett posttest, where untreated control cells served as reference. ns

22 – $p > 0.05$, $*p < 0.05$, $**p < 0.01$, $****p > 0.0001$.

23 **Figure 5. SARS-CoV-2-S furin cleavage site is required for syncytium formation and cell**

24 **entry into TMPRSS2^{+} human cells.**

25 (A) Vero E6, calu-3 and caco-2 cells were infected with pseudotyped VSV harboring VSV-G,

26 wildtype or mutated SARS-CoV-2 spike protein. At 16 h post inoculation, pseudotype entry

1 was analyzed by determining luciferase activity in cell lysates. Signals obtained for particles

2 bearing no envelope protein were used for normalization. The average of three independent

3 experiments is plotted along with ± SEM. (B) (B) Analysis of furin-mediated S protein priming.

4 Rhabdoviral particles harboring the indicated S proteins containing a C-terminal HA-tag for

5 detection were lysed and subjected to Western blot analysis. Detection of vesicular stomatitis

6 virus matrix protein (VSV-M) served as control. (C) Syncytium formation assay: A549-ACE2 or

7 A549-ACE2-TMPRSS2 cells were co-transfected with DsRed expressing plasmid and vector

8 that expressed the indicated S proteins (or no S protein, empty vector, control). At 24 h post-

9 transfection, cells were incubated in the presence or absence of trypsin (1 µg/ml) for 1 h, before

10 they were fixed, stained with DAPI and analyzed by florescent microscopy (scale bars, 100

11 µm).

12 **Figure 6. Heparan sulfate antagonists fails to inhibit SARS-CoV-2 adaptation on Vero E6**

13 **cells.**

14 (A) Vero E6 cells were infected with different SARS-CoV-2 passaged strains at an MOI of

15 0.001 and treated with Surfen or lactoferrin. The supernatant was collected at 24 hpi and

16 titrated on Vero E6 cells. Data are representative of two independent experiments, and each

17 symbol represents biological replicate. Mean and ±SEM is plotted. (B) Vero E6 cells were

18 infected with low or high-passage NK strain viruses. The cells were overlaid with

19 methylcellulose supplemented with 10 µM surfen or 1 mg/mL lactoferrin. The virus plaque size

20 was quantified 3 dpi. Each symbol represents one plaque and data is pooled from multiple

21 infected wells of two independent experiments. (C) NK strain was passaged in Vero E6 cells

22 in the presence of 10 µM surfen. After 4 passages, virus genome sequence was analyzed with

23 deep sequencing. Each symbol represents an individual nucleotide, and genomic positions (x-

24 axis) with mutation frequency >1% are plotted. Red arrows highlight the position of the furin

25 cleavage site and black arrow show synonymous mutation. Statistical significance was

26 calculated using one way ANOVA test and Bonferroni posttest. ns – $p>0.05$, **$p < 0.01$, ****p

27 > 0.0001.

1   **Figure 7. SARS-CoV-2 mutated spike variants are more efficiently cleaved by**

2   **cathepsins.**

3   (A) FAM-TAMRA fret pair coupled S1/S2 spike cleavage site mimetic peptide design. (B)

4   Fluorogenic S1/S2 spike cleavage peptides were cleaved by recombinant proteases and fold

5   increase in FAM florescence is shown. Data is representative of 3 independent experiments,

6   and mean ± SD of 4 replicates is plotted. (C) Peptide cleavage efficiency by different

7   recombinant proteases was measured by calculating area under the curve (AUC) from panel

8   B curves. Replicates from 3 different experiment are shown as mean ± SEM. Statistical

9   significance was calculated with one way ANOVA and Bonferroni posttest. ns – $p>0.05$, ***$p <$

10   0.001, ****$p > 0.0001$.

11

Figure 1
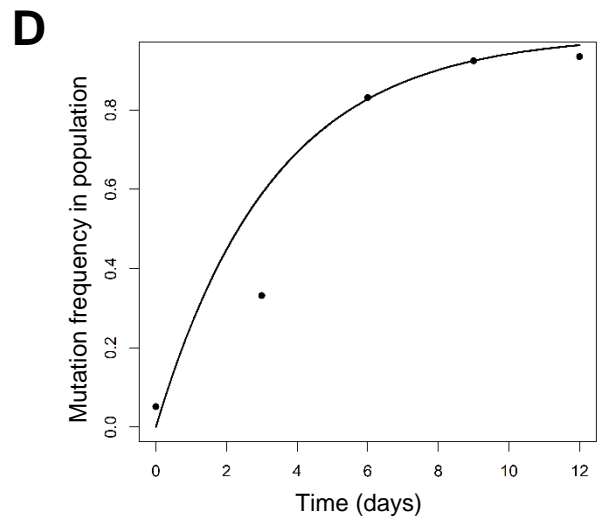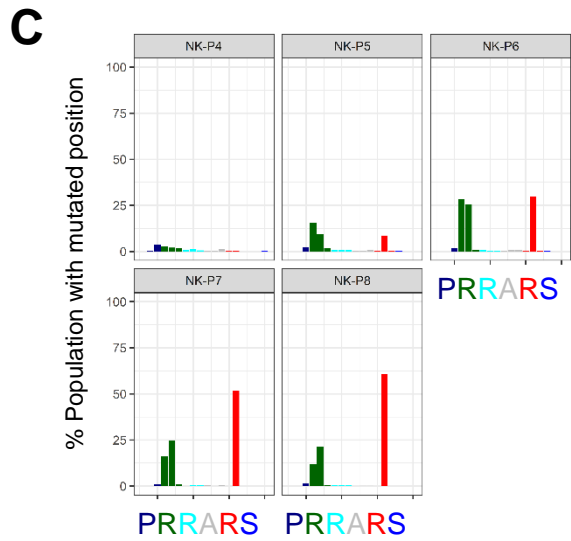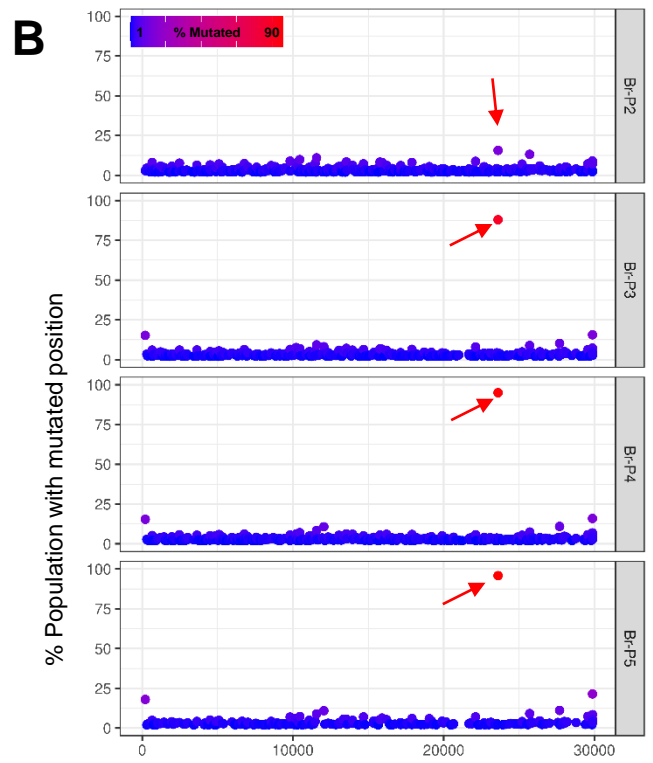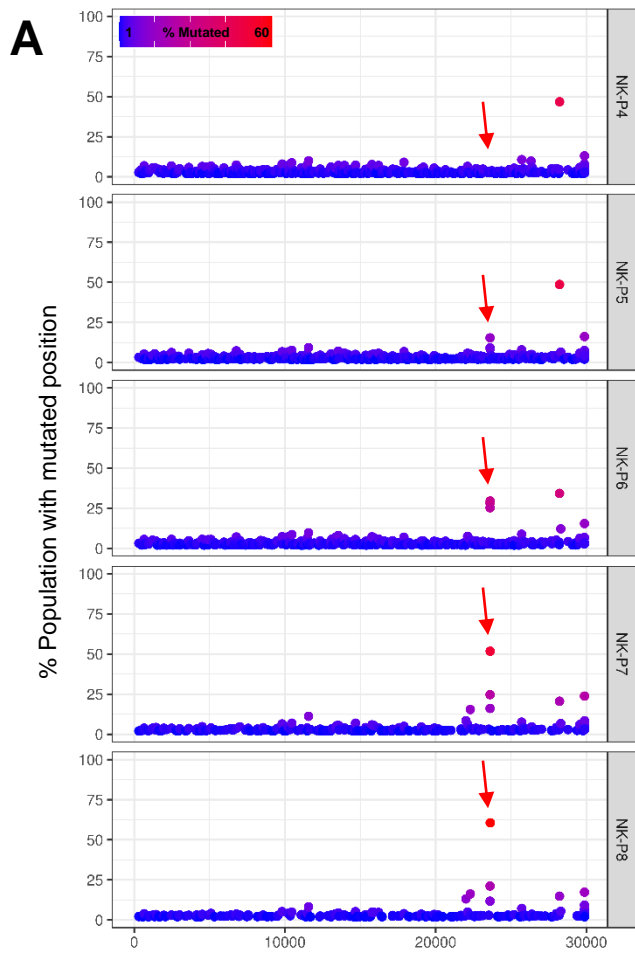
Figure 2

Figure 3

Figure 4

Figure 5

A

Y-axis: Pseudotype Entry [Fold over Background]

Legend:
- VSV-G
- SARS-2-S PRRARS (WT)
- SARS-2-S PWRARS
- SARS-2-S PRRAHS

X-axis: Vero E6, Calu-3, Caco-2

*** **

B

[kDa]

Lanes: Empty Vector, PRRARS (WT), PWRARS, PRRAHS

anti-HA

170
130
100
70
55

● S0 (uncleaved)
● S2 (cleaved)

anti-VSV-M

40
35
25

C

SARS-2-S

| (-) Control | Wildtype | PWRARS | PRRAHS |

A549 (ACE2) — (-) Trypsin

A549 (ACE2) — (+) Trypsin

A549 (ACE2+TMPRSS2) — (-) Trypsin

100 μm
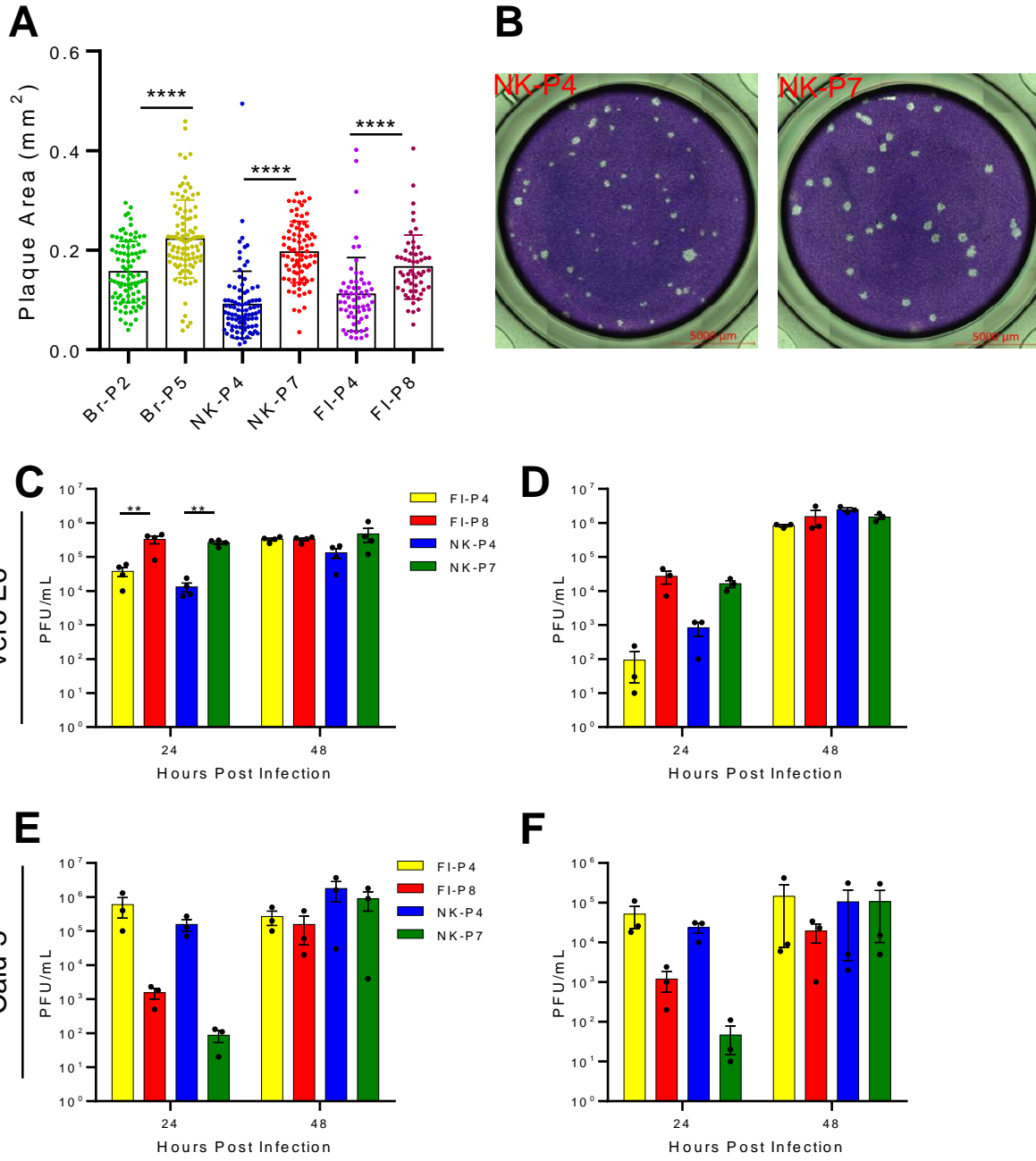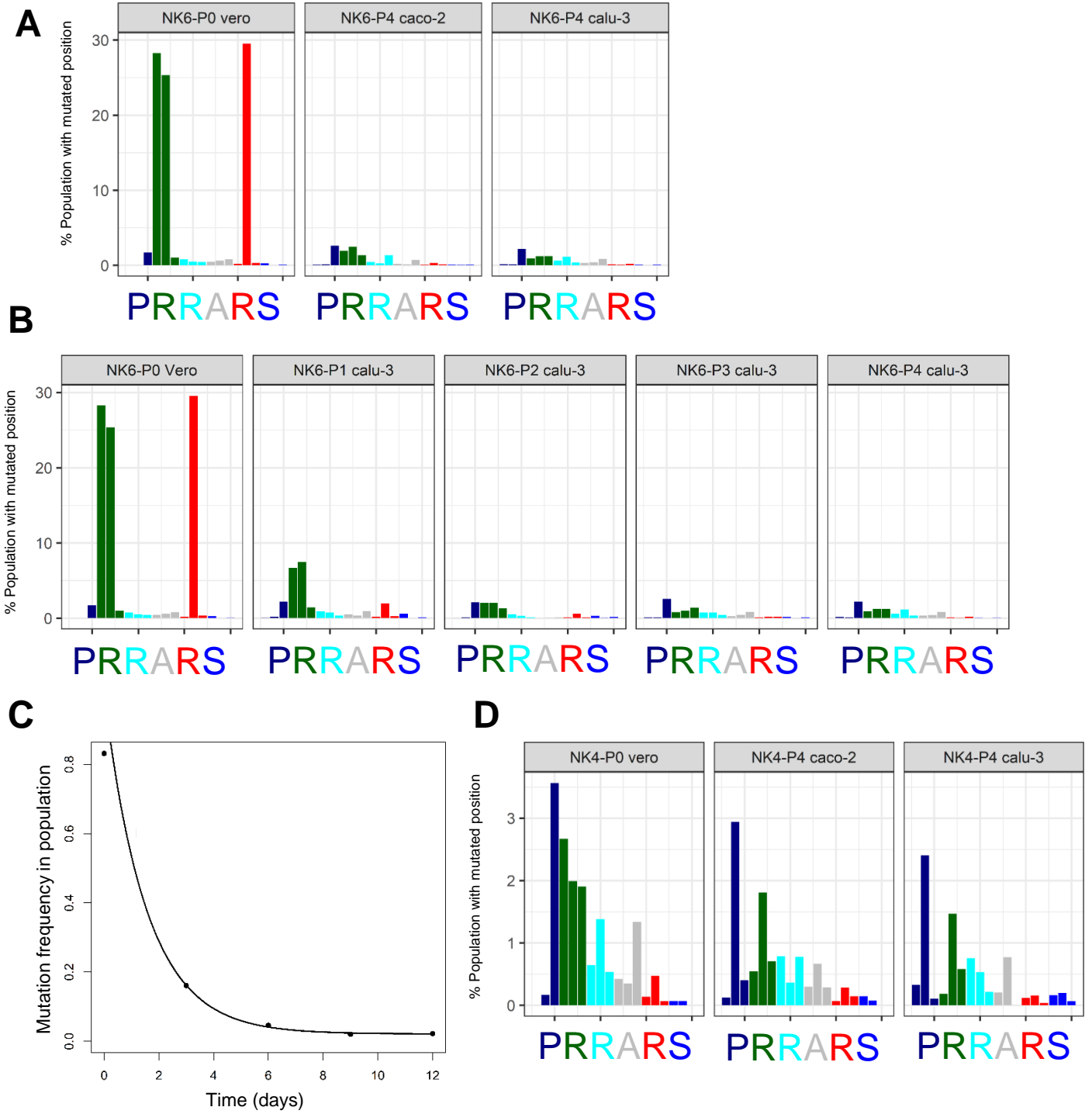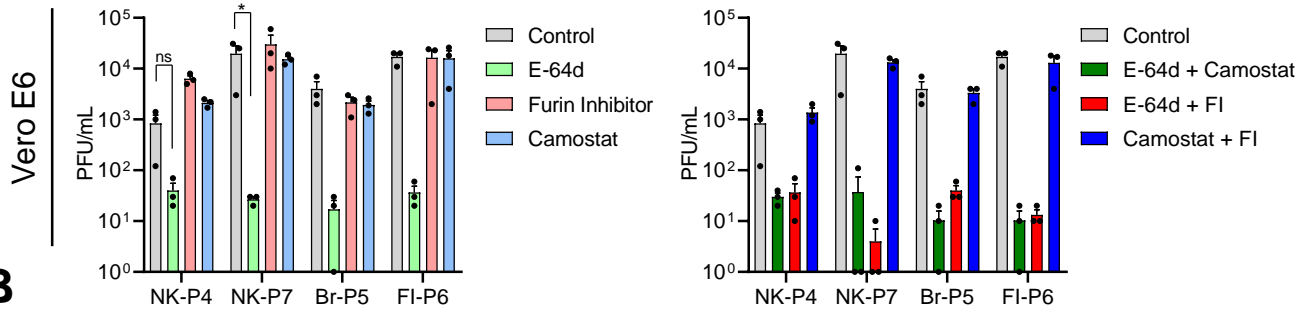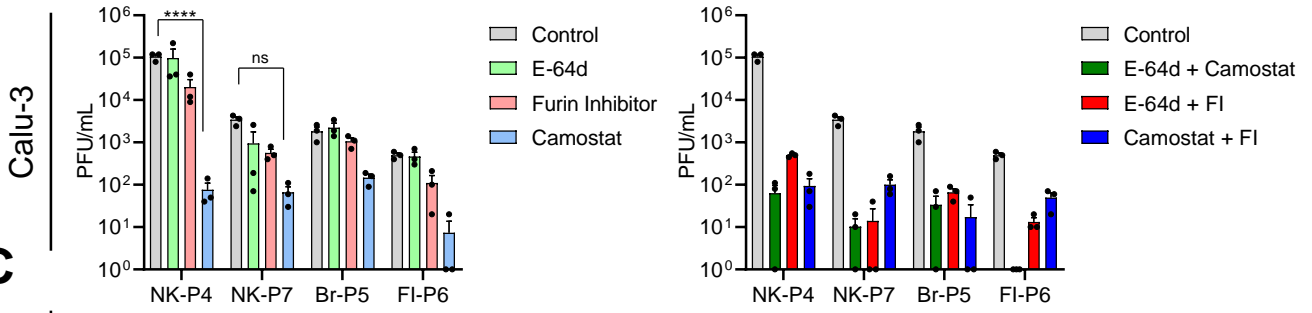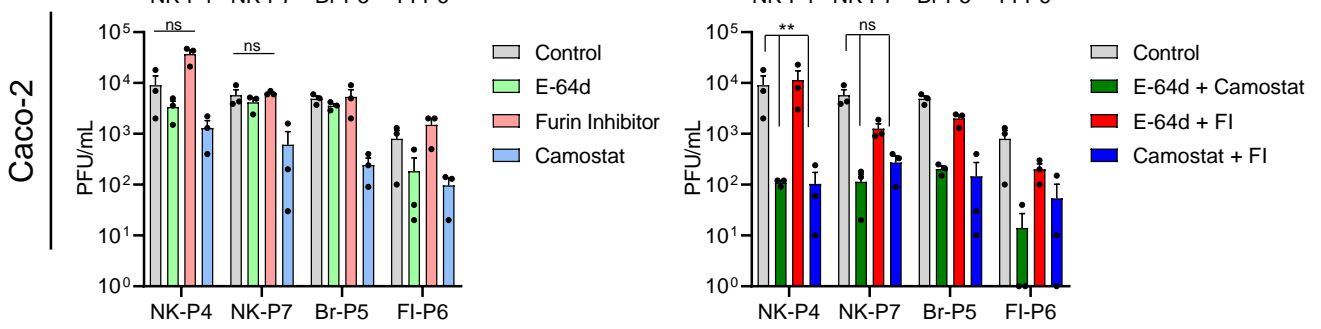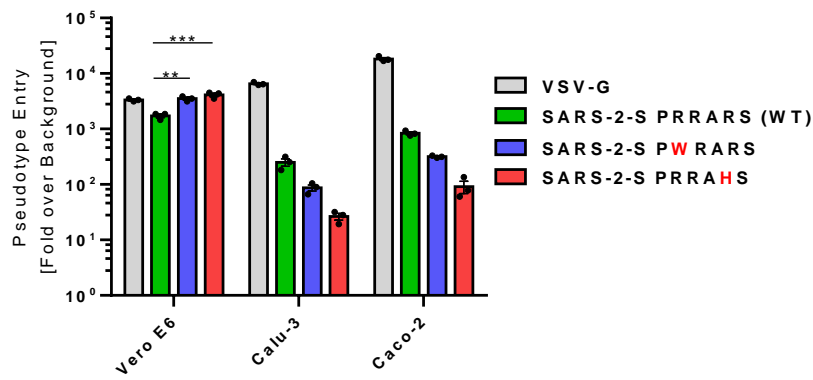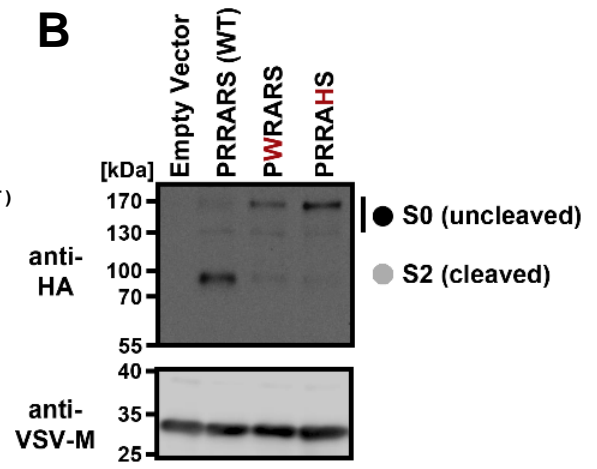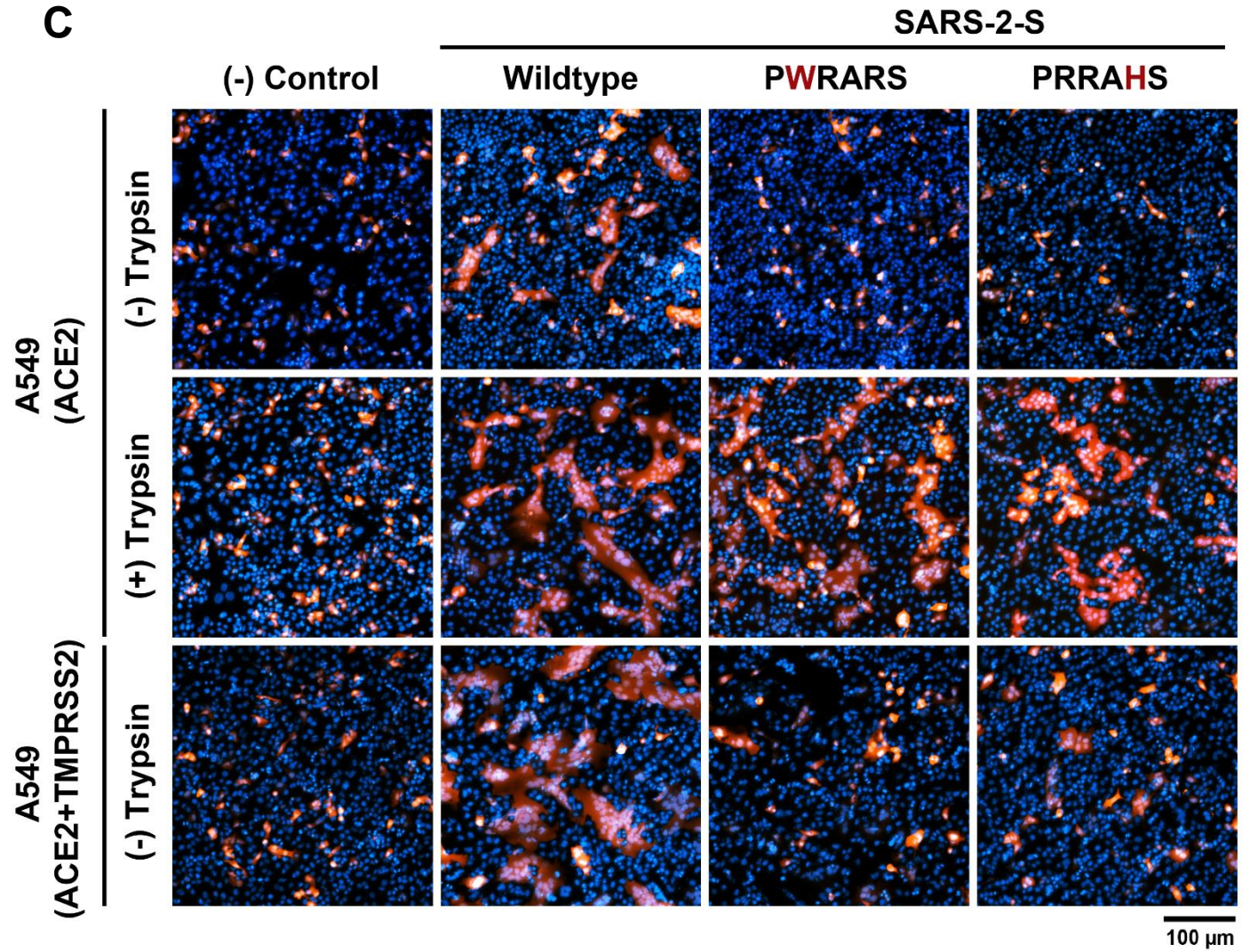
Figure 6

A
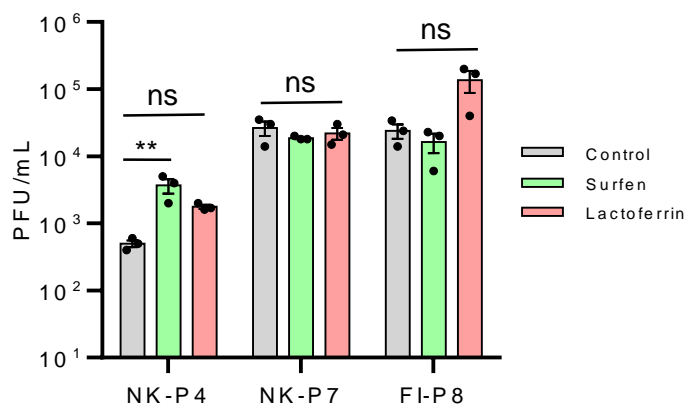
B
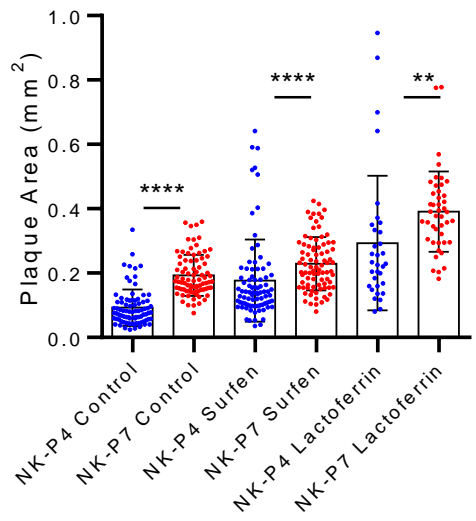
C
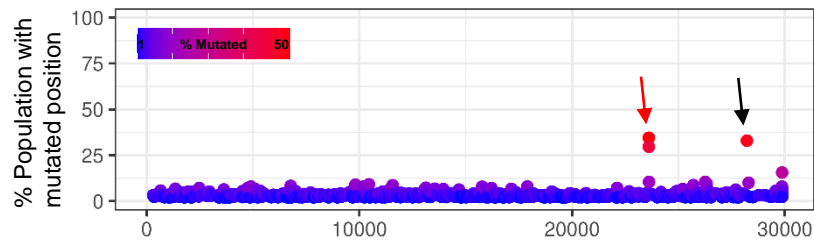
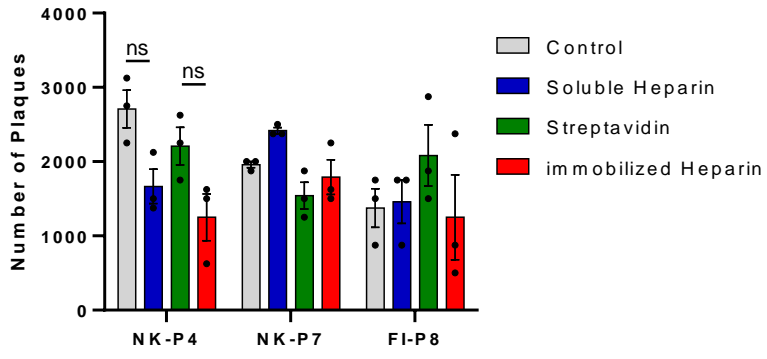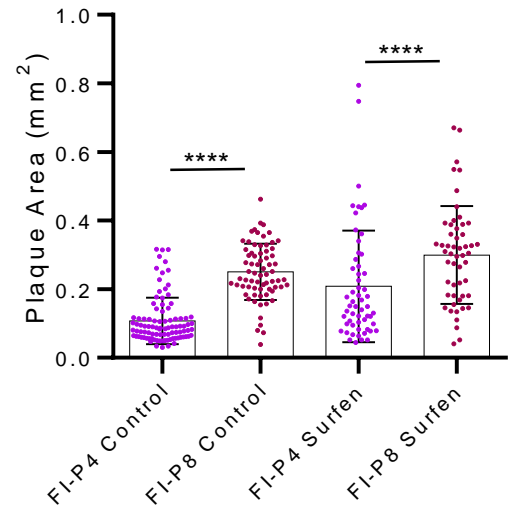# Figure 7

A

B

C

Figure S1

Figure S2

A

B

Figure S3

Figure S4

Figure S5